



Nanoscale structural evolution and phase transformation of geopolymers: *In situ* SAXS/WAXS investigation under uniaxial tension at elevated temperatures



S.A.K.V. Miyurudarshi Piyathilake,*¹ Ivan Kuzmenko, Luckshitha Suriyasena Liyanage, and Christopher Bareither

Accepted: 27 November 2024

Impact statement

This study offers pivotal insights into the degradation mechanisms of high-density polyethylene geomembranes (PE GMXs) through the application of *in situ* SAXS/WAXS techniques. As a crucial material in waste containment infrastructures, PE GMXs' durability is paramount. By simulating real-world exposure conditions (encompassing chemical environments and mechanical stress) in a controlled laboratory setting, we elucidate the structural transformations at micro- and nanoscales within the polymer. Our findings reveal that oxidation-induced chain scission markedly enhances the crystallinity of treated PE GMXs, resulting in a more crystalline and less elastic state. The combined use of FTIR, DSC along with SAXS/WAXS, and simultaneous tensile testing corroborates these structural changes, demonstrating the material's diminished deformation capacity under tensile stress and elevated temperatures. SEM micrographs further illustrate the formation of shish-kebab crystals during high-temperature stretching in chemically and mechanically treated samples, contributing to the increased rigidity of PE GMXs. This comprehensive analysis underscores the critical importance of understanding the chemical and mechanical degradation processes in PE GMXs. The data provided herein are invaluable for improving the durability and performance of geosynthetics in field applications. This innovative approach and detailed findings make a significant contribution to the fields of polymer science and environmental engineering, paving the way for enhanced longevity and reliability of waste containment systems.

This investigation delves into the degradation mechanisms of high-density polyethylene geomembranes (PE GMXs) under a spectrum of conditions, replicating real-world scenarios within a rigorously controlled laboratory setting. The treatment protocols applied induced a notable increase in the crystallinity of the treated specimens relative to the untreated controls. Small-angle x-ray scattering (SAXS) analysis identified an initial long period (interlamellar distance) of 16.9 nm for the untreated polymer, which expanded by 19.5% at a strain of 16.7 percent. Conversely, the treated PE GMXs exhibited a more gradual elongation of the long period, with an increase of merely 10.6% at a strain of 23.3 percent. At an elevated temperature of 65°C, both samples exhibited pronounced strain hardening, with the treated PE GMXs demonstrating superior stability even at a strain of 150 percent. Wide-angle x-ray scattering (WAXS) experiments corroborated these observations, revealing that the diffraction patterns of the untreated PE remained stable up to a strain of 16.7%, whereas those of the treated PE remained distinct up to a strain of 46.1 percent. Scanning electron microscopy (SEM) images substantiated the formation of a shish-kebab structure in the treated samples. The study concludes that the geopolymer underwent oxidation and material degradation as a result of the chemical and mechanical treatments, transitioning to a more crystalline state and concomitantly losing its initial elasticity.

Introduction

Geosynthetics play a crucial role in geoen지니어ing applications across the globe, which include functionality such as filtration, separation, drainage, barrier, and reinforcement.¹ In particular, these versatile materials can be used as impermeable liners in waste containment systems, including municipal, hazardous, and mine waste applications. Commonly used geosynthetics in barrier systems are textured geomembranes (GMXs) and geosynthetic clay liners (GCLs), which

when used together create a robust, composite waste containment solution.^{2–5} The goals of a geosynthetic barrier system are to isolate waste, prevent contaminant release into the environment, and protect human health.¹

A GMX is a thin polymeric film (e.g., 1- to 2-mm thick) primarily composed of polyethylene variants such as high-density polyethylene (HDPE), low-density polyethylene (LDPE), or linear low-density polyethylene (LLDPE). These polyethylene geopolymer materials can experience

S.A.K.V. Miyurudarshi Piyathilake, School of Materials Science and Engineering, Colorado State University, Fort Collins, USA; Miyuru.Piyathilake@colostate.edu

Ivan Kuzmenko, Advanced Photon Source, Argonne National Laboratory, Lemont, USA

Luckshitha Suriyasena Liyanage, Department of Physics, University of Colorado Boulder, Boulder, USA

Christopher Bareither, School of Materials Science and Engineering, Colorado State University, Fort Collins, USA;

Department of Civil and Environmental Engineering, Colorado State University, Fort Collins, USA

*Corresponding author

doi:10.1557/s43577-024-00841-3



progressive material degradation and mechanical property alterations over time, ultimately leading to the potential failure of liner components.⁶ Notably, GMXs are susceptible to oxidative degradation, wherein metal ions present in the surrounding leachates accelerate the generation of free radicals.⁷ The heightened temperatures within waste impoundments, arising from exothermic reactions induced by waste, further exacerbate the oxidation kinetics of geopolymers. Additionally, the substantial mechanical stress resulting from the weight of waste impinges upon the original strength properties of the polymer matrix. The coupled impact of elevated temperatures and mechanical loading can induce significant alterations in the internal molecular architecture of the polymers. Thus, the interplay of chemical surroundings, thermal conditions, and mechanical forces gradually compromises the materials properties of geosynthetic polymers, ultimately affecting their long-term performance.^{8,9}

The goal of this study was to understand the effect of the surrounding solution chemistry, external stress, and heightened temperature on degradation on a high-density polyethylene geomembrane (PE GMX) and to understand and analyze the *in situ* structural transformation within the internal framework of the polymer. This was done to monitor alterations at the nanoscale, with the aim of understanding these changes as they occurred in real time. To achieve this, a controlled laboratory environment was created that simulated the challenging conditions found in real-world contexts and conducted the *in situ* experiments for the exposed PE GMX materials.

The approach of this study involved creating a laboratory-controlled environment to expose PE GMX followed by characterizations. Bauxite-based process solution (B-PS) was synthesized in the laboratory which was specifically designed to mirror the chemical environment encountered at actual bauxite mining sites.¹⁰ To replicate real-world pressures, an external load was applied on the samples, simulating the weight-induced stress. Subsequently, these treated samples were subjected to elevated temperatures and simultaneously performed *in situ* small-angle/wide-angle x-ray scattering (SAXS/WAXS) under tension to understand the real-time structural evolution of HDPE geopolymers. This methodology offered significant insights into the dynamic transformations within these intricate structures under specific conditions.

Background

The structure of a polyethylene-based polymer is typically semicrystalline, composed of both lamellar and amorphous structures. The lamellar structure is formed when polyethylene chains fold to create lamellar crystals, whereas the amorphous structure consists of polymer chains oriented randomly. Factors such as external stress, exposure to chemicals, and high temperatures can modify the initial orientations of the lamellar and amorphous regions, thereby changing their original properties. The SAXS/WAXS technique is an effective method for examining the nanoscale changes in

both amorphous and lamellar crystals within polyethylene.¹¹ The combination of *in situ* SAXS and WAXS is a powerful method to study the hierarchical structure of polymers in real time.¹²

Jiang et al. explored the structural deformation of high-density polyethylene subjected to tensile deformation during annealing.¹³ The authors investigated the structural modifications in polymer under uniaxial tensile stress using the SAXS technique. Key findings include the activation of interlamellar block slips at minor deformations, leading to fragmentation and recrystallization, and the formation of thinner, more stable lamellae. Annealing resulted in the melting of original crystallites and the emergence of distinct lamellar stacks. Notably, lamellae formed during moderate strain stretching remained stable at lower temperatures, only melting at high annealing temperatures. This study illuminates the complex structural changes in HDPE during tensile deformation and annealing, emphasizing the influence of strain, stress-induced processes, and temperature.¹³

Different research examined the structural changes in distinct preoriented isotactic polypropylene (iPP—which is also a polyolefin similar to polyethylene) cast films subjected to uniaxial stretching at room temperature.¹⁴ The study employed *in situ* SAXS/WAXS to explore the transformations induced by stretching. For low-oriented films, the tensile stress induced the amorphization of lamellar crystals parallel to the stretching direction, while the shear stress triggered the shearing of lamellar stacks at other angles through crystal slipping. For high-oriented films, under tensile stress, microbuckling or bending replaced the lamellar shearing to trigger the initial deformation instability of crystals. Stress-induced amorphization of lamellar crystals could also occur at large strains in the strain-hardening zone. This study uncovered the different structural evolution pathways of low- and high-oriented films, which will aid to deepen the understanding of the effects on the deformation mechanisms of other semicrystalline polymers.

Defebvin et al. used x-ray techniques (SAXS/WAXS) to study how poly(vinylidene) fluoride (PVDF) films change when stretched.¹⁵ They found that the crystal phase of PVDF transforms from alpha to beta across all temperatures between the glass transition and melting points, which is key for its electroactive properties. The initial PVDF structure was analyzed using SAXS and WAXS. The patterns showed an isotropic distribution of crystal lamellae and a regular stacking of amorphous and crystalline layers. They have observed the polymer's structural changes and proposed two mechanisms for evaluating crystal structure under stress. First, the alpha–beta crystalline relaxation due to intracrystalline molecular motions significantly impacts PVDF's deformation behavior. Second, in the high-temperature domain, plasticity occurs through crystal block shearing and fibrillation. However, within the alpha–beta transition range, cavitation modes interfere with fibrillation, reducing ductility. The study offers a morphological evolution scheme based on the *in situ*



SAXS/WAXS data to understand PVDF's structural changes upon stretching.

Crystallization under flow is another key concept in polymer deformation, focusing on how flow-induced alignment of polymer chains form “shish” (extended) and “kebab” (folded) structures, especially under extreme environmental conditions such as high temperature and tension.¹⁶ A study by An et al. examined the evolution of gel-spun ultrahigh-molecular-weight polyethylene (UHMWPE) fibers during hot stretching. They used techniques such as *in situ* small-angle x-ray scattering and wide-angle x-ray diffraction measurements to observe structural changes. As stretching strain increased, the fibers' long period increased at lower temperatures. However, at higher temperatures, it has increased initially followed by a rapid decrease. The kebab's thickness remained nearly constant, while the diameter decreased consistently. The formation of shish-kebab structures was identified using SAXS 2D images. The length of shish crystals decreased slightly, while their quantity increased. The degree of crystal orientation remained high throughout the process.¹⁷ These shish-kebab structures significantly enhance the mechanical properties of polymers such as polyethylene, improving their stiffness, strength, and crystallinity.^{18–20} Additionally, factors such as oxidation and crystallinity change further alter polyethylene behavior under extreme environmental conditions. Given that polyethylene geomembranes are exposed to nonstandard chemicals, stress, and elevated temperatures in field conditions, it becomes crucial to study their effects on geopolymer performance, especially in real-time scenarios.

Experimental

Materials and preparation

High-density polyethylene geomembrane (PE GMX) films with 1.6 mm of average thickness were used for this study. The impact of harsh chemical environments and the mechanical stress on the morphological and atomic changes of the polymeric material were evaluated via submerging polyethylene geomembrane films in a laboratory synthesized mine process solution followed by an applied stress at room temperature. Bauxite mine process solution (B-PS) was prepared via procedures in Ghazizadeh et al.¹⁰ to simulate chemical conditions encountered in mine waste containment systems. The recipe for the B-PS is provided in the Supporting information. After

10 months of submersion, the materials were subjected to a normal stress of 2000 kPa to simulate potential stresses acting on the geomaterials in a field application. The polymeric samples tested in this study were collected following the chemical submersion and stress application.²¹ Untreated reference polyethylene samples were obtained at the same time from the same batch, in the as-received conditions, from the polyethylene geomembranes delivered by the manufacturer. The untreated reference sample was aged in normal environmental conditions at 25°C for 10 months.

Following the above experimental procedures, the polyethylene geomembrane samples were subjected to different characterization techniques: Fourier transformation infrared spectroscopy (FTIR), differential scanning calorimetry (DSC), simultaneous small-/wide-angle x-ray scattering (SAXS/WAXS), and tensile testing.

Fourier transformation infrared spectroscopy

A Nicolet iS-50 FT-IR Fourier transform infrared spectrometer with a single pass ATR (diamond and ZnSe crystals) was used to obtain Fourier transformation infrared spectroscopy (FTIR) spectra in both the untreated reference and the treated GMX specimens at room temperature. The spectrometer was set at 4 cm⁻¹ of resolution and each spectrum was averaged over 64 scans. The carbonyl index (CI) and the hydroperoxide/alcohol indices (HI) were calculated as the ratio of the area integrals of the carbonyl peak (1650–1800 cm⁻¹) and hydroperoxide/alcohol peak (3200–3550 cm⁻¹) divided by the C–H peak (1420–1500 cm⁻¹), respectively (Equations 1 and 2).²²

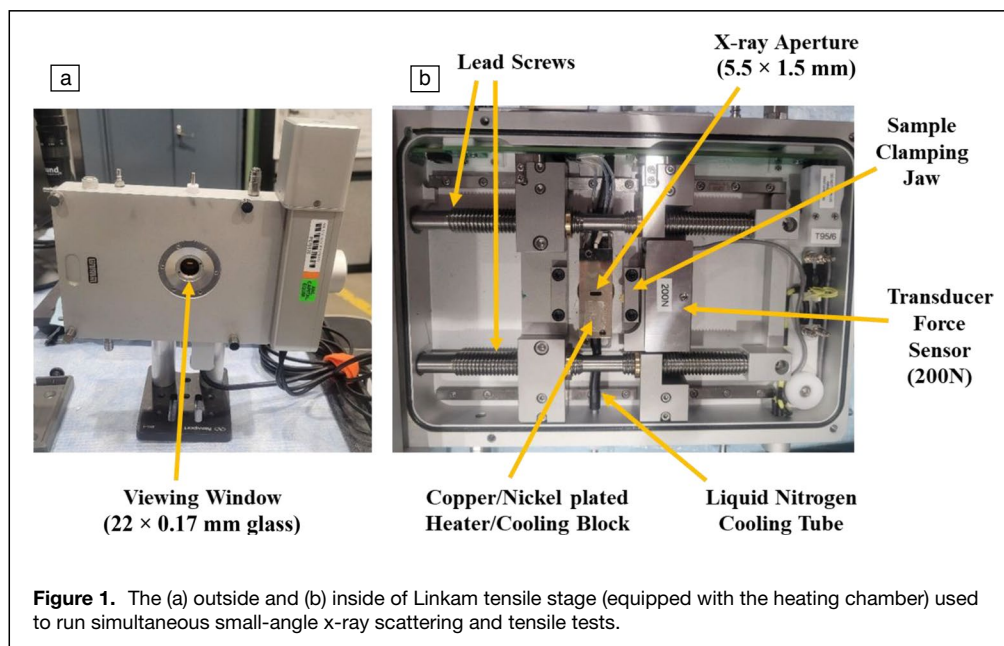
$$\frac{\text{CI Index}}{(\text{Carbonyl compounds})} = \frac{\text{Area under band } 1800\text{--}1600 \text{ cm}^{-1}}{\text{Area under band } 1500\text{--}1420 \text{ cm}^{-1}}, \quad 1$$

$$\frac{\text{HI Index}}{(\text{Hydroperoxide and alcohol})} = \frac{\text{Area under band } 3200\text{--}3550 \text{ cm}^{-1}}{\text{Area under band } 1500\text{--}1420 \text{ cm}^{-1}}, \quad 2$$

Differential scanning calorimetry

Differential scanning calorimetry (DSC) was performed on a DSC 2500 (manufactured by TA Instruments), for thermal analysis and to estimate the degree of crystallinity. The degree of crystallinity (%) was estimated by Equation 3. The heat of fusion of a 100% crystalline polyethylene sample is taken as 293 J/g²³ and the heat of fusion observed in the sample was calculated by integrating the area under the melting peak during the heating curve.²⁴

$$\% \text{Crystallinity} = \frac{\text{Enthalpy of heat of fusion of the PE specimen} \times 100}{\text{Enthalpy of heat of fusion of the 100\% crystalline PE specimen}} \quad 3$$



a control sample), while 65°C simulates the high-temperature conditions geopolymers typically experience in actual use in mining sites.

In mining waste sites, temperatures can vary significantly based on factors such as site depth, geothermal gradient, and environmental conditions. Typically, at relatively shallow depths, temperatures inside a site can exceed 50°C, with the range varying from -27°C to 65°C.^{25,26} Therefore, to represent the structural changes in geopolymers at ambient temperature

and to cover the possible highest field temperatures, 25°C and 65°C were used in this study.

In situ SAXS/WAXS and simultaneous tensile testing

SAXS and WAXS were carried out on the tensile specimens with simultaneous uniaxial PE GMX specimen elongation. SAXS/WAXS measurements were carried out using the Synchrotron radiation (beamline energy range 7–14 keV and usually tuning to 13 keV) at Advanced Photon Source (APS) in the Argonne National Laboratory (Lemont, Ill.). The q range is of 0.002–0.5 Å⁻¹ for 3.6-m camera length and 0.0035–0.9 Å⁻¹ for 2.0-m camera length for SAXS detector (Pilatus 2M) while up to 2.8 Å⁻¹ for WAXS detector (Pilatus 300K). Uniaxial elongation was done using the Linkam tensile stage (TMS600) shown in **Figure 1** with a 200-N load cell. The instrument enabled the sample to be elongated horizontally and symmetrically, ensuring that the x-ray beam always impinged the same area on the sample during the deformation process. The equipment also facilitated heating the specimens enabling testing at elevated temperatures during tensile loading. In this study, PE GMX specimens were tested at room temperature and at 65°C. The initial specimen length between the end clamps was fixed at 50 mm. Deformation was carried out at a constant rate of 5 mm/min to a maximum elongation of 200% of the initial specimen length. Time-resolved x-ray and stress–strain measurements were carried out simultaneously.

The sample-to-detector distance was calibrated using silver behenate. Two-dimensional SAXS and WAXS patterns were recorded every 10 s along with the tensile stress–strain traces. Intensity traces were plotted as a function of the magnitude of the scattering vector q . Untreated PE and the treated PE specimens were tested under the above conditions at 25°C and 65°C. These specific temperatures of 25°C and 65°C for tensile tests were selected to demonstrate different real-world scenarios as 25°C represents ambient temperature (serving as

Results and discussion

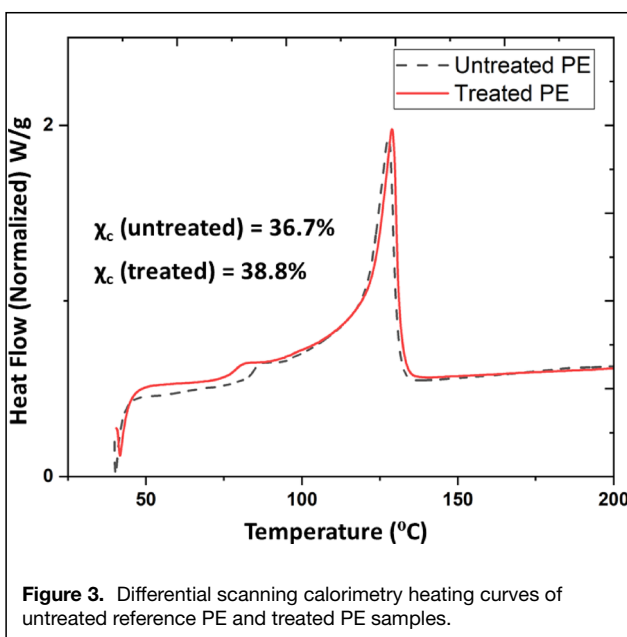
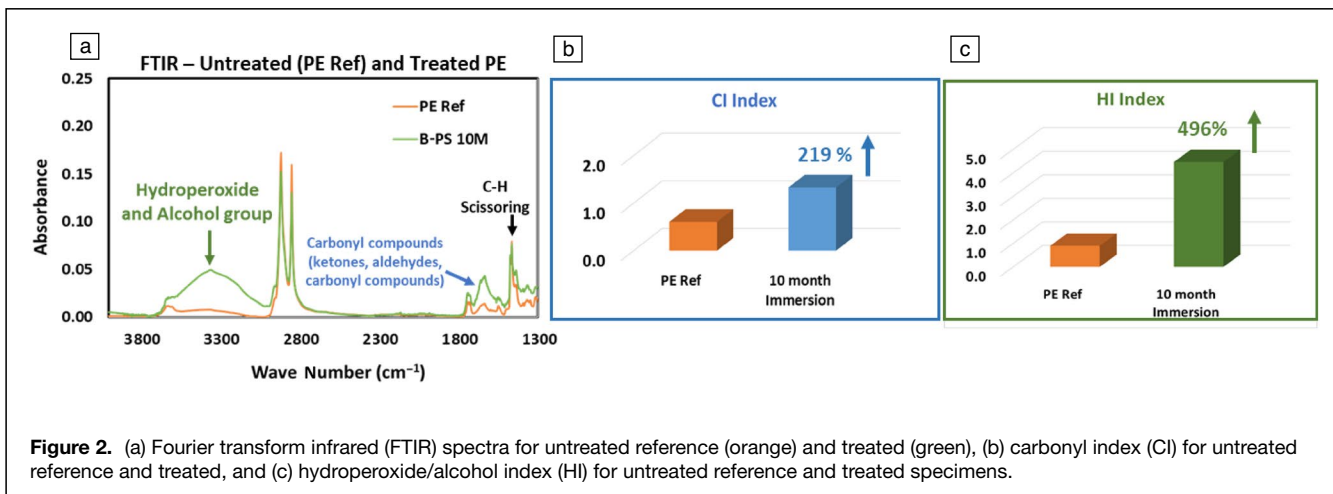
Geopolymer characterization section was divided into two phases: (1) Phase I—understand the effect of solution immersion and stress application on geopolymer degradation, and (2) Phase II—study the structural evolution of the polymer, and associated material changes, with application of external stress at elevated temperatures. Phase I included polyethylene geomembranes that have been exposed to the B-PS solutions and stress and were characterized by FTIR and differential scanning calorimetry (DSC) techniques. Phase II characterization included SAXS/WAXS and tensile strength testing.

Phase I

FTIR

FTIR characterization provides detailed understanding of the chemical changes, functional groups, and structural alterations that occur during polymer oxidation.²⁷ This technique is used to assess the effectiveness of oxidation processes, monitor degradation, and optimize materials properties.

The FTIR spectra for the untreated and treated specimen (i.e., after 10 months of immersion) are shown in **Figure 2a** and the associated bar charts for CI and HI indices for the same two specimens are shown in **Figure 2b–c**. The peaks relevant to hydroperoxide/alcohol (3200–3550 cm⁻¹) and carbonyl compounds (1600–1850 cm⁻¹) increased in intensity after treatment with respect to the untreated polymer. This indicated the treated specimen had undergone oxidation via free radical formation that can generate oxidative products such as hydroperoxides, alcohols, ketones, and carboxylic acid.²⁸ These qualitative



data are quantitatively analyzed by defining CI and HI indices as given in Equations 1 and 2. A 219% increase in the CI index and 496% increase in the HI index were computed for the geomembranes after 10 months of immersion in the B-PS solution and the stress treatment relative to the untreated reference material. These findings indicate that the treatment process increased oxidation in the geopolymer, which can initiate breakdown of the polymer macromolecules and lead to polymer degradation through chain scission.

DSC

The DSC thermograms of the untreated PE and treated PE are shown in Figure 3. The curves present the heating cycles and the endothermic melting peaks of both specimens. The crystallinity of the treated specimen (computed via Equation 3) increased by 5.8% relative to the untreated PE. This observation, combined with FTIR results, suggests that the chain

scission mechanism was dominant in the treated polymer. Free radical formation via oxidation can induce chain scission that can increase the crystallinity of the polymer.^{29–31}

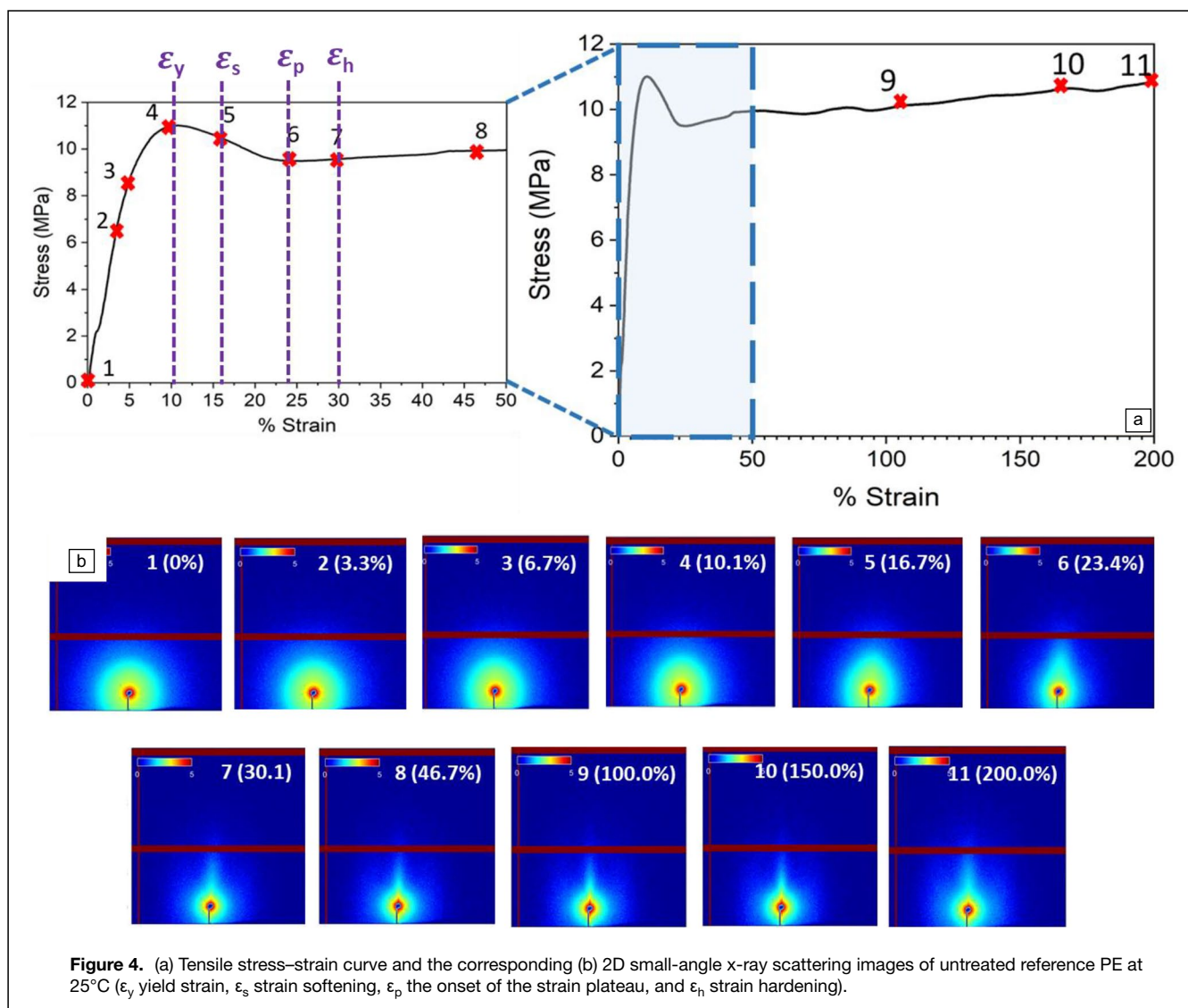
This chain scission process is enhanced by the externally applied tensile stress, which can accelerate the degradation process of polymers. The presence of tensile stress separates radicals formed from the newly broken molecule and prevents recombination, which would potentially cause an increase in chain scission. Furthermore, the applied stress can enhance alignment of the polymer chains and could induce strain crystallization to heighten crystallinity.^{32,33} Considering the analysis from both FTIR and DSC findings, the geopolymer underwent oxidation, chain scission, and material degradation due to the chemical and mechanical exposures. Consequently, the geopolymer evolved into a state with higher crystallinity. A higher crystallinity implies increased stiffness and reduced elasticity. This suggests that the geopolymer loses its initial elasticity after exposure, a characteristic crucial for comprehending deformation under applied load in field applications.

Phase II

SAXS with simultaneous tensile stress at 25°C

The 2D SAXS images from 0% strain to 200% strain at 25°C for the untreated PE and associated stress–strain curve constructed by the Linkam tensile stage during the simultaneous tensile test are shown in Figure 4. The 2D images are numbered from b (1) to b (11) with corresponding strain values and are stated in the top right-hand corner of each image. In addition, the relevant positions for 1–11 images are marked in the tensile stress–strain curve. The first portion of the stress–strain behavior to 50% strain is magnified and shown to the left of the complete stress–strain curve. Finally, distinct regions representing yield strain (ϵ_y), strain softening (ϵ_s), the onset of the strain plateau (ϵ_p), and strain hardening (ϵ_h) are identified in the tensile stress–strain curve.¹⁴

The 1D plots of Intensity versus q are presented in Figure 5. These plots were derived from the corresponding 2D images where the process involved integrating the intensity of each 2D image over a complete circle (360° azimuthal angle), starting from



the beam center and extending radially outward along the \mathbf{q} vector. A 1D curve for a specific strain is obtained by integrating the 2D image that corresponds to the particular strain. All the intensity versus \mathbf{q} value curves that were integrated from the relevant 2D images (from 0% to 150% strain) are shown in Figure 5a. The peak at the \mathbf{q} value $\sim 0.4 \text{ \AA}^{-1}$ is constantly visible in all the plots and that originates from the machine setup. The squared area of Figure 5a is magnified and presented as in Figure 5b.^{14,34,35}

The initial 2D SAXS image of the untreated PE at 0% strain exhibits isotropic characteristics and appears bright as shown in Figure 4b. This isotropic SAXS pattern corresponds to the signal of spherulites with macroscopically homogenized and randomly oriented structure of lamellae. The particular 1D curve for 0% strain (as shown in Figure 5a) is used to determine the interlamellar distance, also known as the long period (L_p), using Equation 4.

According to Figure 5b, at 0% of tensile strain, the \mathbf{q}_{peak} is equal to 0.037 \AA^{-1} . Thus, the initial long period (L_p) of the untreated PE at 25°C is 16.9 nm (using Equation 4).^{11,15,36,37}

$$\text{Long period (interlamellar distance)} = L_p = \frac{2\pi}{q}. \quad 4$$

During the stretching process, the peak intensities of the 2D images remain relatively stable, showing no significant alterations up to a strain of 10.0 percent. However, when the strain reaches 16.7%, a noticeable decrease in intensity begins to manifest in both 2D and 1D representations as depicted in Figures 4 and 5. The initial isotropic representation has evolved into an anisotropic state and exhibits compression along the meridional direction. At this deformation stage, the \mathbf{q}_{peak} has reduced down to 0.031 \AA^{-1} and the long period has raised up to 20.2 nm (19.5% increase) indicating the occurrence of lamellar separation and an extension of the interlamellar amorphous in meridional direction.³⁶

After that, in the strain softening zone, the lamellae along the stretching direction undergo more separation as indicated by the continuous increase of the long period. After the strain

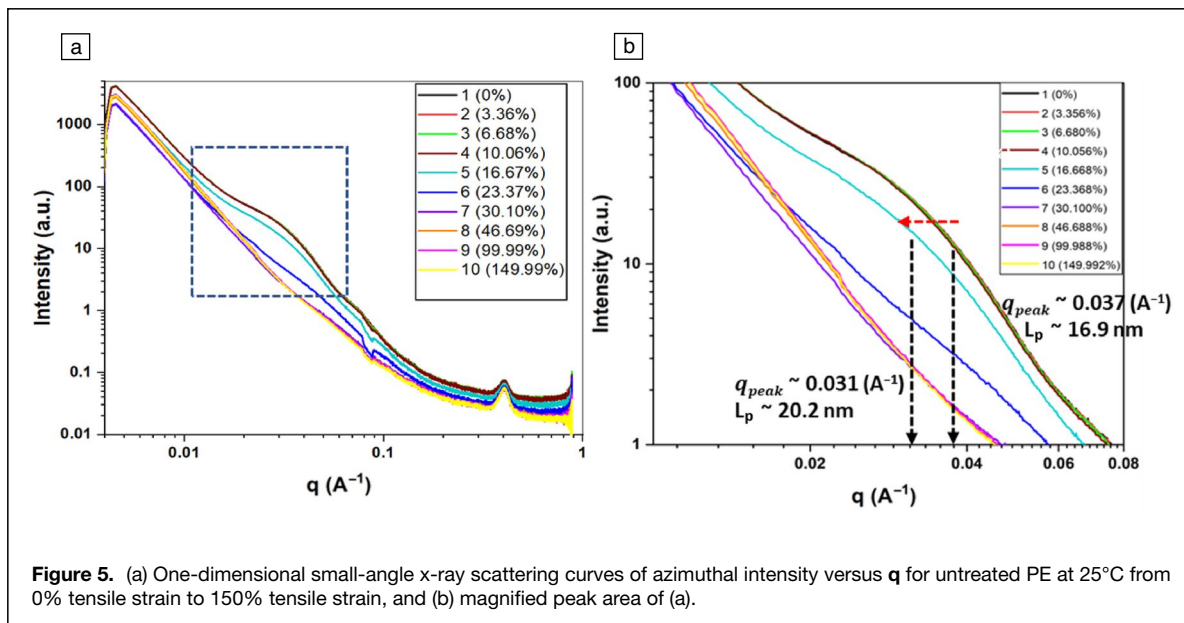


Figure 5. (a) One-dimensional small-angle x-ray scattering curves of azimuthal intensity versus q for untreated PE at 25°C from 0% tensile strain to 150% tensile strain, and (b) magnified peak area of (a).

plateau, strain hardening begins; however, the slope of the strain hardening appears to be quite minimal. As the material enters the strain-hardening phase, a sudden decrease in the long period is observed in the 1D curve (Figure 5b), particularly after reaching 23.3% strain. This observation is clearly visible in the 2D SAXS image at 23.3% strain (Figure 4) as well. The deformation of the 2D representation has further intensified, and the signal intensities in the meridional direction have undergone additional compression. This suggests an accelerated disintegration of the lamellar structure under the applied tensile stress. Around 30.1% strain, an equatorial streak signal appears in the 2D SAXS patterns. This phenomenon suggests that under that particular range of tensile strain the lamellar stacks break into blocks through pulling out chains from crystals, which promotes the formation of microfibrils.³⁸ This is further confirmed by a fast decrease of the SAXS azimuthal intensity.

Contrasting with Figure 5, **Figure 6** includes both the collection of 2D SAXS images and the corresponding 1D curves for both the untreated PE and the treated PE during stretching from 0% to 150 percent. Those 2D SAXS images and the corresponding 1D curves in Figure 6 compare the structural evolution of untreated versus treated PE specimen under uniaxial tension at 25°C. Upon application of tensile stress, the treated PE sample demonstrated a slower propagation of the long period extension compared to the untreated reference PE. This behavior is clearly visible in Figure 6a–b. The intensity of the q_{peak} decreased more rapidly in the untreated sample (16.7%) compared to the treated sample (23.3%).

This suggests a higher resistance to deformation in the treated sample. Moreover, the long period at a strain of 23.3% for the treated sample was measured to be 18.7 nm (10.6% increase), whereas it was 20.2 nm for the untreated sample at a strain of 16.6 percent. This indicates that the treated polymer has less deformation of the lamellae

compared to the untreated polymer. Supporting this observation, the 2D SAXS images showed a noticeable distortion of image isotropy at a strain of 23.3% for the untreated samples, while this distortion was only observed at a strain of 46.6% for the treated sample signifying that the lamellar separation is slower in the meridional direction. This observation is further corroborated by the rapid decrease of the q_{peak} intensity at a strain of 46.68% in the treated sample, compared to a strain of 23.3% for the untreated PE, as depicted in Figure 6b–c 1D curves.

The preceding analysis indicates that the treated PE exhibits less structural deformation and increased rigidity following treatment. This could be attributed to the effects of oxidation and applied stress, which have influenced the crystallinity and molecular structure orientation, culminating in a highly oriented crystal structure in the treated polymer.

The pronounced orientation of lamellae and chains in the treated polymer inhibits the deformation of the lamellae structure at the initial stages of uniaxial stretching. Consequently, the treated polymer exhibits reduced elasticity compared to the untreated reference PE. This could be interpreted as a degradation of the polymer materials, given that these materials are engineered to resist and preserve a specific level of elasticity.

SAXS with simultaneous tensile stress at 65°C

The same experimental procedure carried out for treated and untreated samples at 25°C was followed at 65°C to assess the geopolymer structural evolution at elevated temperatures. The samples were stretched at 65°C and the stress–strain trace along with the corresponding 2D SAXS images of untreated and treated polymers is shown in **Figure 7a(i)** and **b(i)**. Corresponding 2D images for the untreated and treated PE at 65°C stretching are shown in Figure 7a(ii) and **b(ii)**₁ and **b(ii)**₂. Both samples at 65°C stretching show prominent strain hardening

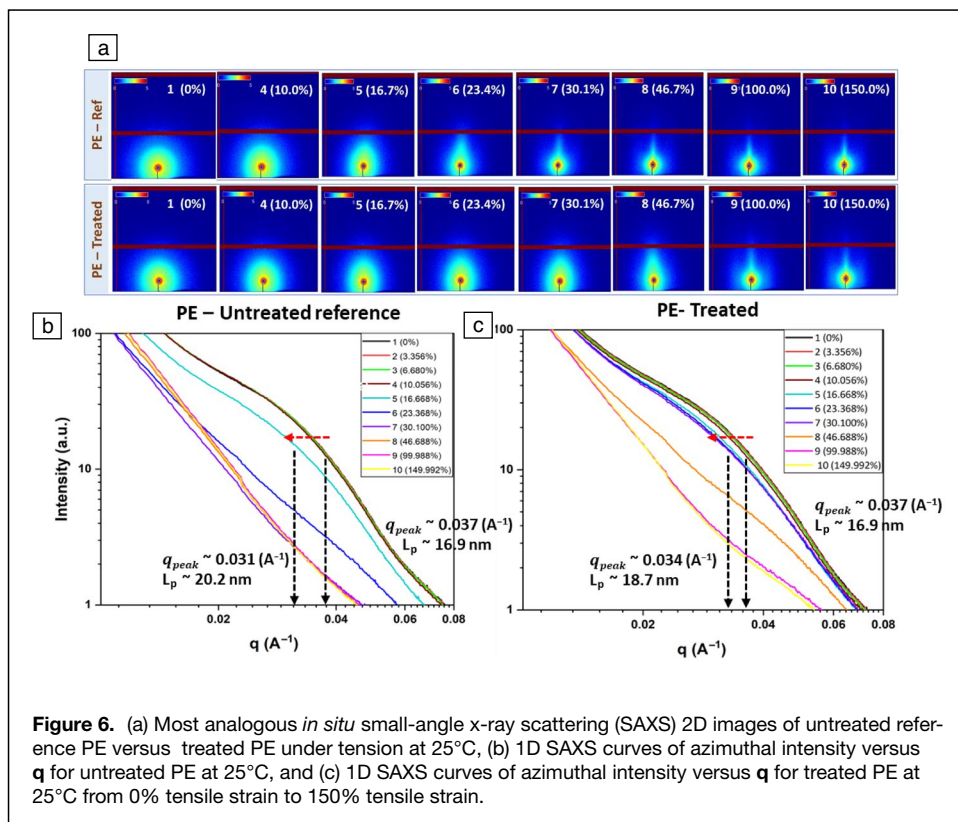


Figure 6. (a) Most analogous *in situ* small-angle x-ray scattering (SAXS) 2D images of untreated reference PE versus treated PE under tension at 25°C, (b) 1D SAXS curves of azimuthal intensity versus q for untreated PE at 25°C, and (c) 1D SAXS curves of azimuthal intensity versus q for treated PE at 25°C from 0% tensile strain to 150% tensile strain.

compared to the samples stretched at 25°C. The reason could be that the higher temperatures enhance the mobility of polymer chains, promote recrystallization, and facilitate secondary bonding, all of which contribute to strain hardening.^{39–42}

Similar to the observations made for 25°C, the changes in the isotropic 2D SAXS patterns can be attributed to the breaking of lamellae by stretching (Figure 7). In general, for both treated and untreated samples, the characteristic SAXS streaks appear in the equatorial direction of 2D SAXS patterns at higher strains than the 25°C stretching.

However, in the 2D SAXS images of both samples, we observe the emergence of a new peak. Alongside the equatorial streak signal, two newly formed two-point signals appear in the meridional direction. These scattering signals likely originate from periodically alternating kebab lamellae with an intermediate amorphous region at heightened temperature.^{43–45} Also, the applied strain leads to the formation of fibrillar shish, composed of stretched chains aligned along the flow direction.⁴³ The formation and evolution of shish-kebab crystals can primarily be achieved through lamellar fragmentation and crystal slip at the stretching temperature of 65°C. At very high stretching temperatures, they are potentially achieved via stress-induced melting and recrystallization. As the stretching temperature increases, crystals orient more easily, and the fibrillar crystals formed at high temperatures are superior to those formed at low temperatures due to partial chain disentanglement.⁴⁶

In this study, the B-PS and stress-treated specimen begins forming the new structure at approximately 46% strain,

whereas the reference PE sample shows this behavior at around 99% strain. This difference may be attributed to an increased degree of macromolecular orientation, favoring easier crystallization in the treated polymer due to B-PS solution and stress exposure. These findings are further supported by the 1D curves shown in Figure 8. The corresponding new peak appears at $q \sim 0.045 \text{ (}\text{\AA}^{-1}\text{)}$ in the 1D curves.

SEM analysis and comparison

The SEM and the corresponding 2D SAXS images of (b(i)) reference PE at 0% strain at 25°C (b(ii)) untreated PE at 200% strain at 65°C (b(iii)) treated PE at 200% strain at 65°C are shown (Figure 9). The SEM

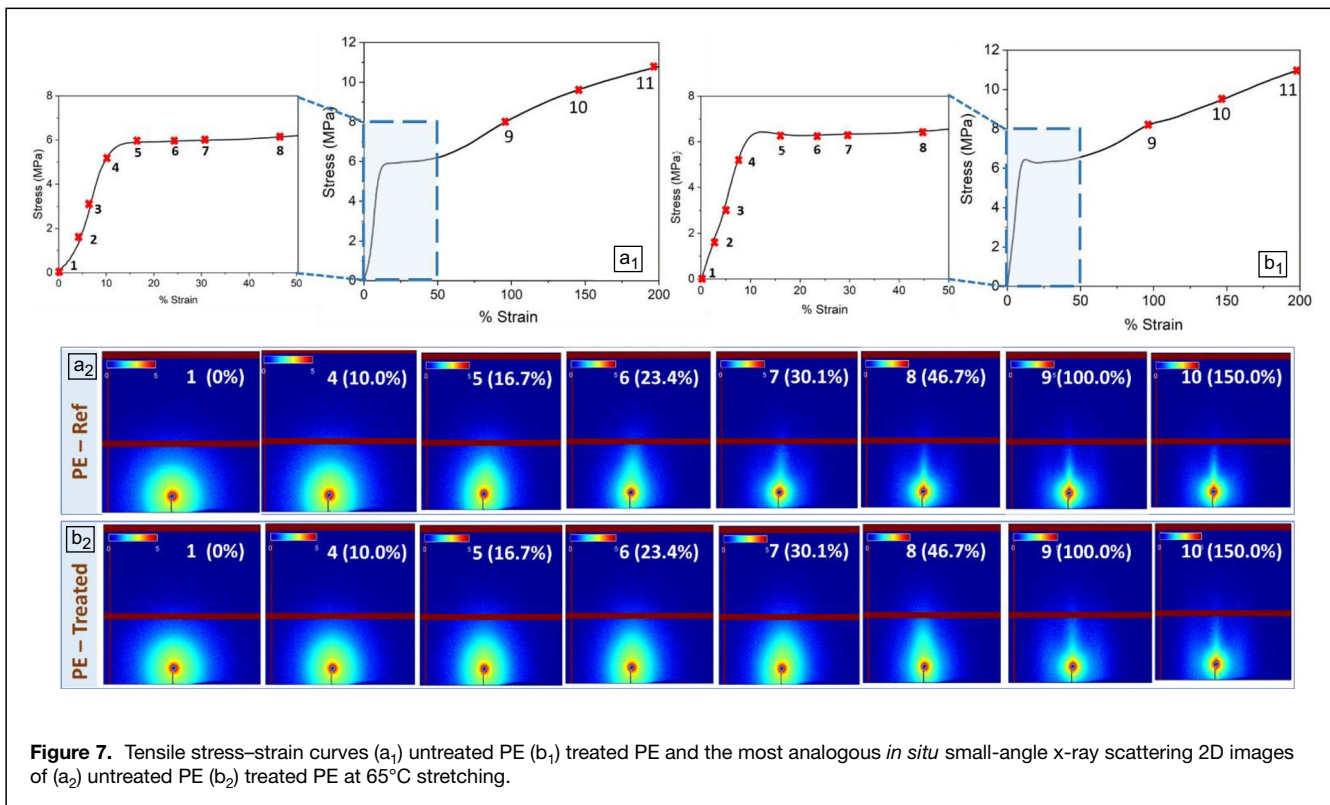
images effectively highlight the development of a shish-kebab structure at 65°C.

A noticeable variation of the shish-kebab densities of this structure is clearly evident when comparing samples that have undergone treatment and stretching at 65°C to those that were untreated and stretched at 65°C. This observation underscores and verifies the findings gathered through the SAXS and concurrent tensile investigations.

WAXS with simultaneous tensile stress

Two-dimensional WAXS images of both untreated and treated PE subjected to strain ranging from 0% to 150% at 25°C and 65°C are presented in Figure 10. WAXS images were collected simultaneously with the SAXS data. Due to the concurrent WAXS/SAXS acquisition mode, the range of the collected WAXS data does not span the full 360° azimuthal angle; it is less than that.⁴⁸

At 0% strain, two isotropic circles are discernible, representing the congruent diffraction patterns for HDPE. From the inner circle outward, the diffraction circles correspond to the (110) plane and (200) plane of the orthorhombic crystals in HDPE.⁴⁹ Upon the application of tension to the polymer, alterations in the crystalline structure result in a smearing of the WAXS crystalline peaks. As previously discussed, PE is a semicrystalline polymer, characterized by regions where chain segments align parallel to each other, forming crystalline lamellae, interspersed with large amorphous areas exhibiting



random orientation. The application of tension forces these chains to reorient, disrupting the crystalline structure and causing the WAXS peaks to distort and blur.^{50–52}

Both the (110) and (200) crystal planes of the untreated and treated specimens exhibit more intense diffraction rings initially. In the untreated PE, the diffraction patterns remain stable until 16.7% of strain, corresponding to the end of the yield region as per the tensile traces provided in Figure 4. Subsequent to this point, the diffraction patterns blur, potentially indicative of fragmented crystals. In the later stages of stretching, the diffraction signal transitions from diffraction arcs to short arcs, suggesting that a significant number of crystals align along the direction of stretching under higher strain. At approximately 150% of stretching, the arcs further shorten, implying that the crystals are more neatly oriented along the direction of stretching. For the treated PE, the diffraction peaks do not smear up to 46.1% of applied strain, indicating a more resilient crystal structure post-treatment, as discussed in the SAXS analysis as well. This observation highlights the resistance of the crystal structure to deformation following the treatment process which would not be ideal for geopolymers in the field.

At 65°C, as shown in Figure 10c–d, the diffraction peaks corresponding to the crystalline planes are more stable than those at 25°C. Among all the samples, the PE treated at 65°C exhibits the highest stability, as the crystalline peaks remain undeformed and undistorted even under higher strains. Even at a strain of 150%, the arc-like diffraction pattern

for the 110 plane is still observable. The presence of the shish–kebab structure, as discussed in previous sections, could be the reason for this behavior.

Summary

This study investigates the degradation of high-density polyethylene geomembranes (PE GMXs), a geosynthetic used in waste containment, under various conditions. The real-world exposure conditions, including chemical environment and mechanical stress, were simulated in a laboratory setting and analyzed structural transformations within the polymer at micro- and nanoscales. The treatment process increased oxidation in the geopolymer, leading to polymer degradation through chain scission. This was confirmed through Fourier transformation infrared spectroscopy (FTIR) and differential scanning calorimetry (DSC) techniques. The results showed an increase in the crystallinity of the treated specimen by 5.8% relative to the untreated reference PE, suggesting a dominant chain scission mechanism. The applied stress enhanced this process, leading to a more crystalline state in the geopolymer and a loss of its original elasticity. Following this, the research employed SAXS/WAXS characterization to examine the structural changes in both untreated and treated PE. These examinations were conducted at temperatures of 25°C and 65°C under concurrent tensile stress. The rationale for this approach is that it can simulate the dynamic conditions these materials encounter in real-world settings, including high temperatures and stresses.

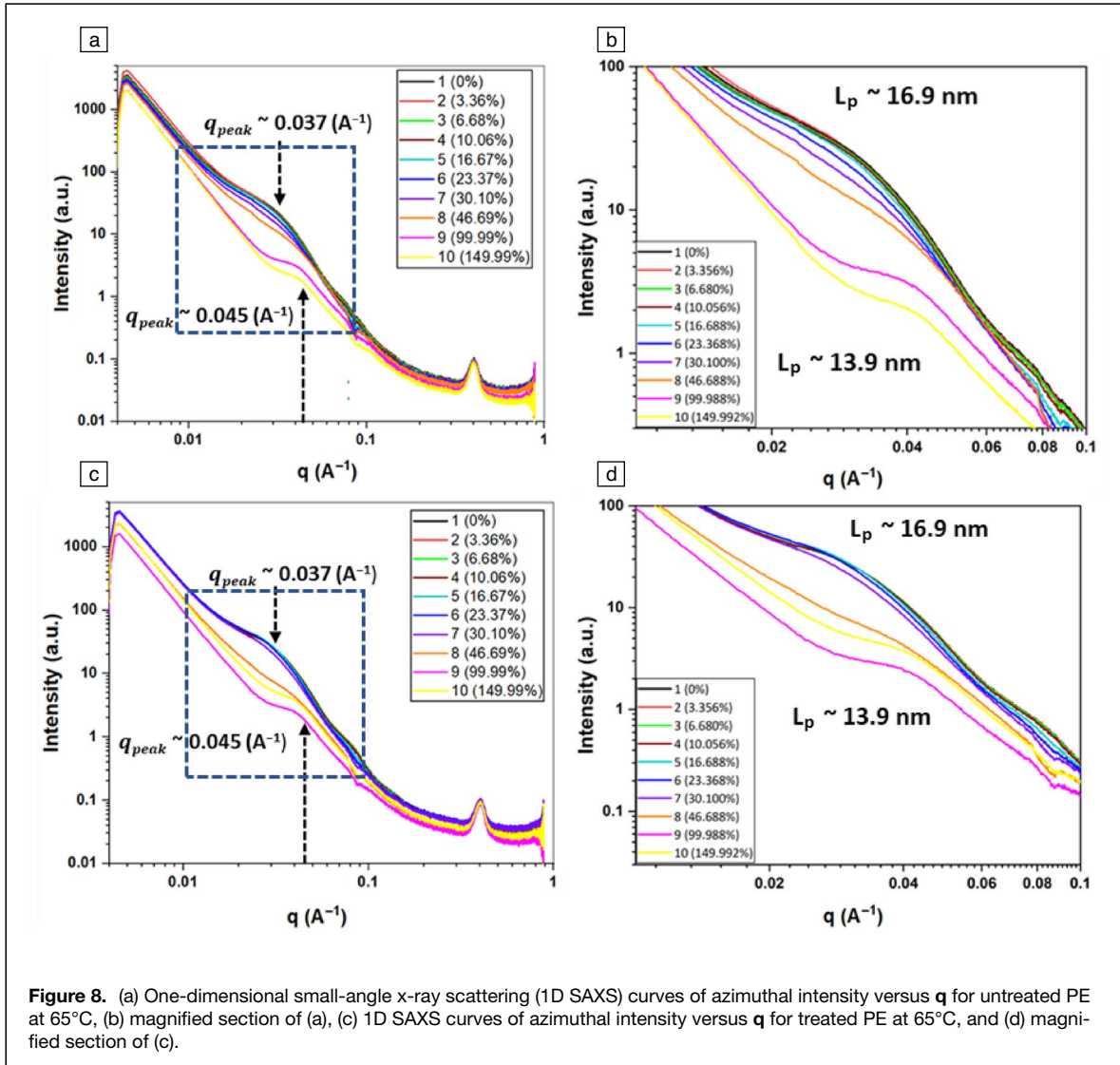


Figure 8. (a) One-dimensional small-angle x-ray scattering (1D SAXS) curves of azimuthal intensity versus q for untreated PE at 65°C, (b) magnified section of (a), (c) 1D SAXS curves of azimuthal intensity versus q for treated PE at 65°C, and (d) magnified section of (c).

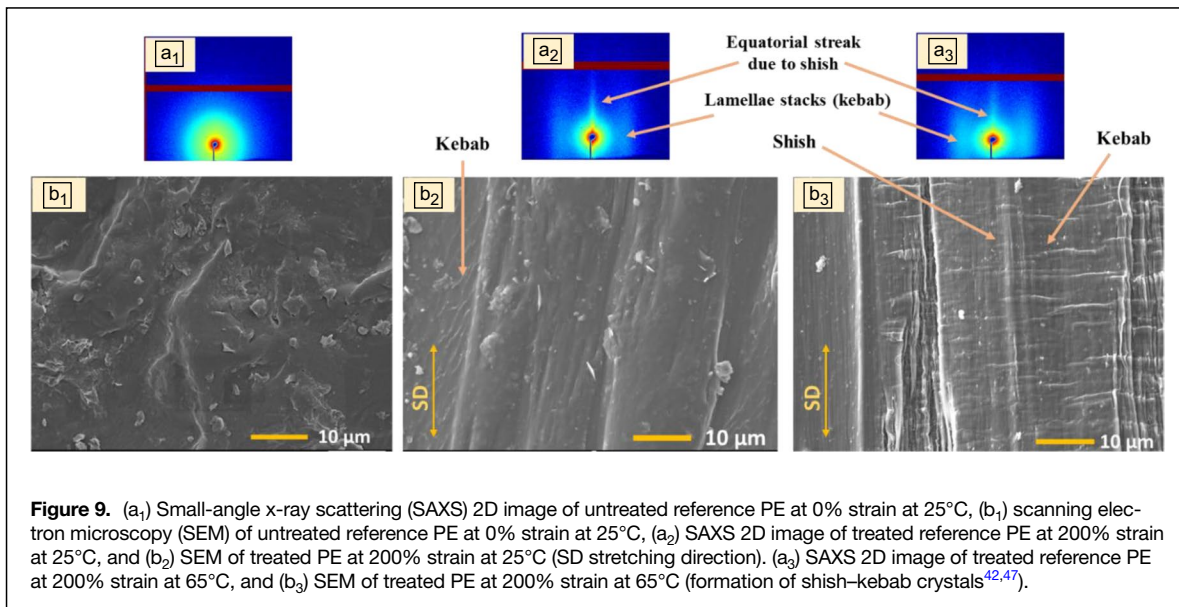


Figure 9. (a₁) Small-angle x-ray scattering (SAXS) 2D image of untreated reference PE at 0% strain at 25°C, (b₁) scanning electron microscopy (SEM) of untreated reference PE at 0% strain at 25°C, (a₂) SAXS 2D image of treated reference PE at 200% strain at 25°C, and (b₂) SEM of treated PE at 200% strain at 25°C (SD stretching direction). (a₃) SAXS 2D image of treated reference PE at 200% strain at 65°C, and (b₃) SEM of treated PE at 200% strain at 65°C (formation of shish-kebab crystals^{42,47}).

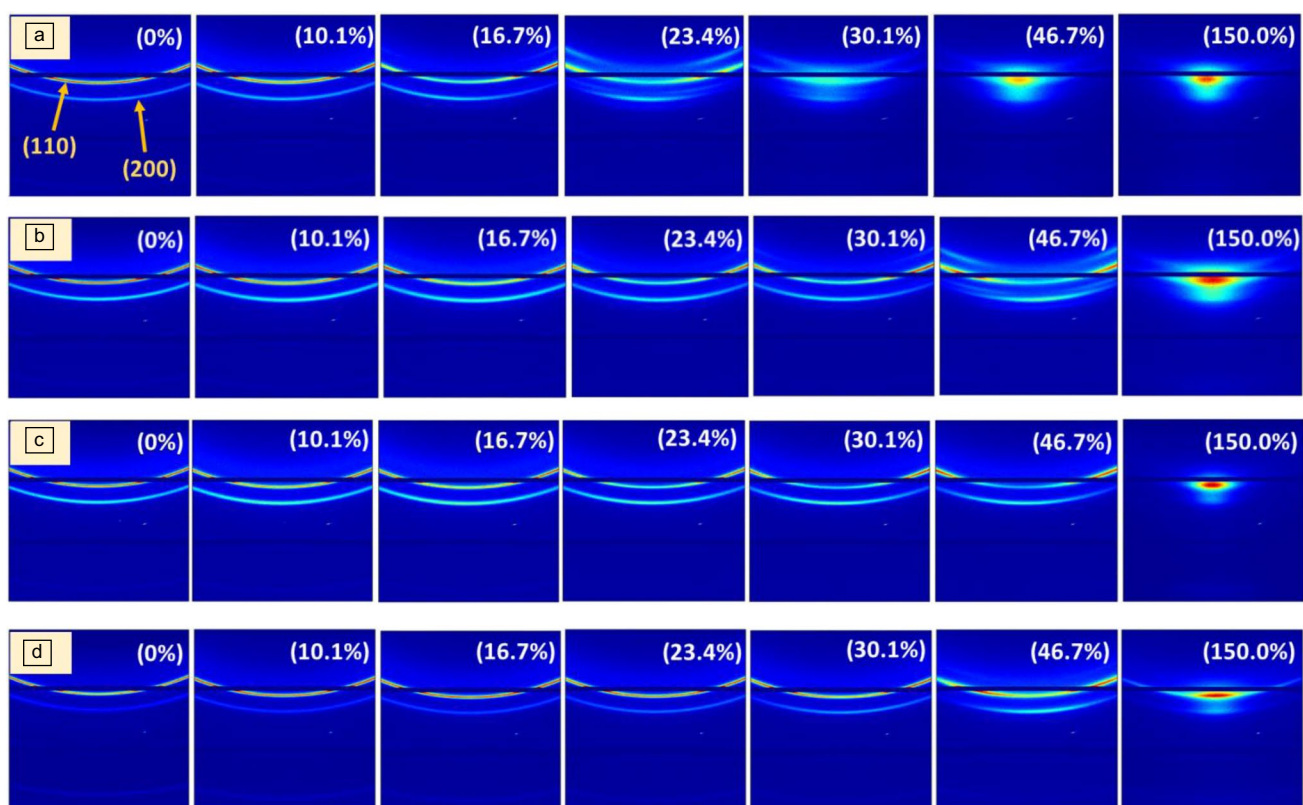


Figure 10. Wide-angle x-ray scattering two-dimensional (WAXS 2D) images of (a) untreated reference PE at 25°C, (b) treated PE 25°C, (c) untreated reference PE at 65°C, and (d) treated PE 65°C from 0% to 150% strain.

The initial long period (L_p) of the untreated PE was 16.9 nm. During stretching at 25°C, the peak intensity remained stable up to a strain of 10.0%, but at 16.7% strain, the meridional intensities of the 2D images decreased, and the long period increased to up 20.2 nm (19.5% increase). Around 30.1% strain, an equatorial streak signal appeared in the 2D SAXS patterns, suggesting the lamellar stacks break into blocks, promoting the formation of microfibrils. The treated PE demonstrated a slower propagation of the long period extension compared to the untreated PE. The long period at a strain of 23.3% for the treated sample was 18.7 nm (10.6% increase), whereas it was 20.2 nm for the untreated sample at a strain of 16.6 percent. This indicates that the treated polymer has a lower capacity to deform under the extension compared to the untreated polymer at 25°C.

At 65°C, both samples showed prominent strain hardening compared to the samples stretched at 25°C, likely due to enhanced mobility of polymer chains and recrystallization facilitated at higher temperatures. Changes in the isotropic 2D SAXS patterns, similar to observations made for 25°C, were attributed to the breaking of lamellae by stretching, after the elastic region. Characteristic SAXS streaks appeared in the equatorial direction of 2D SAXS patterns at higher strains than the 25°C stretching for both samples.

However, a new peak emerged in the 2D SAXS images of both samples, with two newly formed two-point signals appearing in the meridional direction, likely originating from periodically alternating kebab lamellae with an intermediate amorphous region at heightened temperature. The B-PS and stress-treated specimen began forming this new structure at approximately 46% strain, whereas the reference PE sample showed this behavior at around 99% strain. SEM analysis illustrated the formation of a shish-kebab structure in the treated specimen, with a distinct difference in densities from the untreated specimen at 65°C.

At a temperature of 25°C, the WAXS tests on both untreated and treated PE samples, which were under tensile stress at 0% strain, revealed two isotropic circles. These circles represented matching diffraction patterns discernible for HDPE. Upon the application of tension, alterations in the crystalline structure resulted in a smearing of the WAXS crystalline peaks. The diffraction patterns of the untreated PE remained undistorted until 16.7% of strain, after which they blurred, potentially indicative of fragmented crystals. For the treated PE, the diffraction peaks did not smear up to 46.1% of applied strain, indicating a more resilient crystal structure post-treatment. At 65°C, the diffraction peaks corresponding to the crystalline planes were more stable than

those at 25°C. The treated PE at 65°C exhibited the lowest deformation, with the crystalline peaks remaining undistorted even under higher strains. Even at a strain of 150%, the arc-like diffraction pattern for the 110 plane was still observable. The presence of the shish-kebab structure could be the reason for this behavior.

In essence, the findings are crucial for understanding the chemical and mechanical degradation of PE geopolymer in field applications. The geopolymer has transitioned into a more crystalline state with exposure to the chemical and mechanical exposure and the treated PE exhibits superior strain tolerance and increased rigidity following the treatment process, which could be attributed to the effects of oxidation, applied stress, and high-temperature effects. This transformation implies a loss of the original elasticity in the geopolymer postexposure, which could be interpreted as a degradation of the polymer material because it is a property important in understanding deformation under applied load in field applications.

As the experimental results and findings indicate that geopolymers become less elastic and stiffer, it can potentially reduce the durability of the polymers. Stiffer materials are more susceptible to cracking and breaking under stress, leading to premature failure and necessitating frequent replacements. This increases operational costs and downtime and can compromise the structural integrity of the site. Failures of geopolymers may result in increased environmental contamination and pollution if not managed properly.^{53,54} Stiffer materials may not provide the necessary elasticity, support, and stability required to withstand and hold the pressure of the waste, potentially leading to failures.

Conclusions

- The study found that the B-PS and stress treatment process led to an increase in oxidation within the geopolymer. This oxidation process resulted in the degradation of the polymer through a mechanism known as chain scission, which involves the breaking of the polymer chains that was further enhanced by the applied tension. On the other hand, the stress can align the crystals and increase the crystallinity. Both of those degradation mechanisms were confirmed using Fourier transformation infrared spectroscopy (FTIR) and differential scanning calorimetry (DSC) techniques. This led to a more crystalline state in the geopolymer and resulted in a loss of its original elasticity. This loss of elasticity is significant as it affects the geopolymer's ability to deform under applied load in field applications.
- The SAXS analysis of the untreated and treated PE under simultaneous tensile stress at 25°C revealed that the initial long period (L_p) of the untreated PE was 16.9 nm. During the stretching process, the peak intensity of the 2D images remained stable up to a strain of 10.0%, but at 16.7% strain, the meridional intensity decreased, and the

long period increased to 20.2 nm. The treated PE demonstrated a slower propagation of the long period extension compared to the untreated PE, indicating a lower capacity of the treated polymer to deform under the extension. The SAXS experiments conducted on the treated and untreated PE samples under simultaneous tensile stress at 65°C showed that both samples exhibited prominent strain hardening compared to the samples stretched at 25°C.

- At 65°C, both samples showed more strain hardening than at 25°C due to increased polymer chain mobility and recrystallization. Changes in the 2D SAXS patterns were similar to those at 25°C, attributed to lamellae breaking from stretching. A new peak in the 2D SAXS images indicated a new structure formation at higher strains, likely from alternating kebab lamellae with an amorphous region at higher temperature. The B-PS and stress-treated sample started forming this structure at around 46% strain, while the untreated PE sample did so at about 99% strain. The formation of a shish-kebab crystal structure in treated PE was confirmed by SEM observations.
- WAXS experiments conducted on the treated and untreated PE samples simultaneously with SAXS, at 25°C and 65°C revealed that at 0% strain, two isotropic circles representing the congruent diffraction patterns for HDPE were discernible. Upon the application of tension, alterations in the crystalline structure resulted in a smearing of the WAXS crystalline peaks. The diffraction patterns of the untreated PE remained stable until 16.7% of strain, after which they blurred, potentially indicative of fragmented crystals. For the treated PE, the diffraction peaks did not smear up to 46.1% of applied strain, indicating a more resilient crystal structure post-treatment.
- The study concludes that the geopolymer experienced oxidation and material degradation following the chemical and mechanical treatments. As a result, the geopolymer transitioned into a more crystalline state. This transformation implies a loss of the original elasticity in the geopolymer postexposure, a property important to understanding deformation under applied load in field applications. This understanding is crucial for the effective use of high-density polyethylene geomembranes in waste containment and other field applications.

Acknowledgments

This work was supported in part by the School of Advanced Materials Discovery (SAMd) and its Research Core Facility (RRID: SCR_022002) at Colorado State University (CSU). S.A.K.V.M. Piyathilake was supported in part by a Geosynthetic Institute (GSI) Fellowship. We also extend our gratitude to Nipa Khair for fruitful discussions. Most of the analytical work was performed at Colorado State University Analytical Resources Core (ARC) Facility, RRID: SCR_021758 and the Advanced Photon Source at Argonne National Laboratory.



Author contributions

S.A.K.V.M.P. contributed toward investigations and writing—original draft; I.K. contributed toward investigations and writing—original draft; L.S.L. contributed toward investigations and writing—original draft; and C.B. contributed toward writing—review and editing, supervision, project administration, and funding acquisition.

Data availability

Data will be made available on request.

Conflict of interest

The authors declare that they have no known competing financial interests or personal relationships that could have appeared to influence the work reported in this paper.

Supplementary information

The online version contains supplementary material available at <https://doi.org/10.1557/s43577-024-00841-3>.

References

- R.M. Koerner, in *Designing with Geosynthetics*, 5th edn., ed. by R.M. Koerner (Prentice Hall, Hoboken, 2005)
- R.K. Rowe, M.S. Morsy, A.M.R. Ewais, *Waste Manag.* **100**, 18 (2019). <https://doi.org/10.1016/j.wasman.2019.08.028>
- S. Vahidi, G. Hsuan, A. ElSafty, *Geotext. Geomembr.* **48**(2), 170 (2020). <https://doi.org/10.1016/j.geotexmem.2019.11.009>
- T. Bauters, "Geotextiles in Waste Containment," In *Geotextiles: From Design to Applications* (Elsevier, Amsterdam, 2016)
- A.J. Puppala, A. Banerjee, S.S.C. Congress, "Geosynthetics in Geo-infrastructure Applications," in *Durability of Composite Systems* (Woodhead Publishing, 2020), pp. 289–312. <https://doi.org/10.1016/B978-0-12-818260-4.00007-7>
- J.H. Greenwood, H.F. Schroeder, W. Voskamp, *Part 2: Durability of Geosynthetics*, vol. 33, no. 5 (2015). <https://geosyntheticsmagazine.com/2015/10/01/part2-durability-of-geosynthetics/>
- Y. Hsuan, H. Schroeder, R.K. Rowe, W. Miller, J. Greenwood, D. Cazzuffi, R. Koerner, "Long-Term Performance and Lifetime Prediction of Geosynthetics," in *Proceedings of the 4th European Conference on Geosynthetics (EuroGeo 2008)* (2008), pp. 1–40. <https://www.semanticscholar.org/paper/LONG-TERM-PERFORMANCE-AND-LIFETIME-PREDICTION-OF-Hsuan-Schroeder/5098e4606b93a143ab69fd902ed3f50eac826bde>
- R.K. Rowe, T. Mukunoki, R.J. Bathurst, S. Rimal, P. Hurst, S. Hansen, *Geotext. Geomembr.* **25**(2), 68 (2007). <https://doi.org/10.1016/j.geotexmem.2006.10.003>
- R.K. Rowe, M.Z. Islam, Y.G. Hsuan, *Geosynth. Int.* **15**(2), 136 (2008). <https://doi.org/10.1680/gein.2008.15.2.136>
- S. Ghazizadeh, C.A. Bareither, J. Scalia, C.D. Shackelford, *J. Geotech. Geoenviron. Eng.* **144**(10), 06018011 (2018). [https://doi.org/10.1061/\(asce\)gt.1943-5606.0001953](https://doi.org/10.1061/(asce)gt.1943-5606.0001953)
- S. Kanomi, H. Marubayashi, T. Miyata, H. Jinnai, *Nat. Commun.* **14**(1), 5531 (2023). <https://doi.org/10.1038/s41467-023-41138-4>
- Y. Lin, W. Chen, L. Meng, D. Wang, L. Li, *Soft Matter* **16**(15), 3599 (2020). <https://doi.org/10.1039/c9sm02554e>
- Z. Jiang, Y. Tang, Y. Men, H.-F. Enderle, D. Lilge, S.V. Roth, R. Gehrke, J. Rieger, *Macromolecules* **40**(20), 7263 (2007). <https://doi.org/10.1021/ma0627572>
- J.C. Habumugisha, S. Feng, O. Iqbal, Y. Lin, M. An, L. Meng, D. Wang, W. Chen, L. Li, *Polymer* (Guildford) **214**, 123234 (2021). <https://doi.org/10.1016/j.polymer.2020.123234>
- J. Defebvin, S. Barrau, G. Stoclet, C. Rochas, J.M. Lefebvre, *Polymer* (Guildford) **84**, 148 (2016). <https://doi.org/10.1016/j.polymer.2015.12.041>
- M. An, Y. Lv, G. Yao, L. Zhang, Z. Wang, *J. Polym. Sci. B Polym. Phys.* **56**(3), 225 (2018). <https://doi.org/10.1002/polb.24517>
- D. Mi, C. Xia, M. Jin, F. Wang, K. Shen, J. Zhang, *Macromolecules* **49**(12), 4571 (2016). <https://doi.org/10.1021/acs.macromol.6b00822>
- B. Chen, J. Gong, J. Zhang, C. Deng, X. Gao, *Mater. Today Commun.* **38**, 107911 (2024). <https://doi.org/10.1016/j.mtcomm.2023.107911>
- H. Zheng, Y. Quan, G. Zheng, K. Dai, C. Liu, C. Shen, *RSC Adv.* **5**(74), 60392 (2015). <https://doi.org/10.1039/C5RA07453C>
- J. Zhang, Y. Zhang, Y. Li, M. Luo, J. Zhang, *Polymers* (Basel) **16**(8), 1032 (2024). <https://doi.org/10.3390/polym16081032>
- S. Ghazizadeh, C.A. Bareither, "Effect of Mine Process Solutions on the Internal Shear Strength of Geosynthetic Clay Liners," *Geo-Congress 2020: Engineering, Monitoring, and Management of Geotechnical Infrastructure (GSP 316)* (Minneapolis, February 25–28, 2020), pp. 619–628. <https://doi.org/10.1061/9780784482797.060>
- J. Almond, P. Sugumaar, M.N. Wenzel, G. Hill, C. Wallis, *e-Polymers* **20**(1), 369 (2020). <https://doi.org/10.1515/epoly-2020-0041>
- R.L. Blaine, *Thermal Applications Note: TNO48 Polymer Heats of Fusion* (TA Instruments, New Castle, 2002), pp. 1–2
- TA Instruments, *Thermal Analysis Application Brief: Determination of Polymer Crystallinity by DSC* (TA Instruments, New Castle, n.d.)
- S. Hardcastle, "Cooling Canada's Mines," *Canadian Mining Journal* (October 1, 2019)
- N. Yeşiller, J.L. Hanson, E.H. Yee, *Waste Manag.* **42**, 166 (2015). <https://doi.org/10.1016/j.wasman.2015.04.004>
- U. Riaz, S.M. Ashraf, "Characterization of Polymer Blends with FTIR Spectroscopy," in *Characterization of Polymer Blends* (Wiley, Weinheim, 2015), pp. 625–628.
- E. Smidt, M. Schwanninger, *Spectrosc. Lett.* **38**(3), 2147 (2005)
- P. Bracco, L. Costa, M.P. Luda, N. Billingham, *Polym. Degrad. Stab.* **155**, 67 (2018). <https://doi.org/10.1016/j.polymdegradstab.2018.07.011>
- S. Yamamoto, T. Kubo, K. Satoh, *J. Polym. Sci.* **60**(24), 3435 (2022). <https://doi.org/10.1002/pol.20220250>
- Y.K. Song, S.H. Hong, S. Eo, W.J. Shim, *Environ. Pollut.* **327**, 121590 (2023). <https://doi.org/10.1016/j.envpol.2023.121590>
- S. Humbert, O. Lame, G. Vigier, *Polymer* (Guildford) **50**(15), 3755 (2009). <https://doi.org/10.1016/j.polymer.2009.05.017>
- K.S. Simis, A. Bistolfi, A. Bellare, L.A. Pruitt, *Biomaterials* **27**(9), 1688 (2006). <https://doi.org/10.1016/j.biomaterials.2005.09.033>
- W. Du, Y. Ren, Y. Tang, Y. Shi, X. Yao, C. Zheng, X. Zhang, M. Guo, S. Zhang, L.-Z. Liu, *Eur. Polym. J.* **103**, 170 (2018). <https://doi.org/10.1016/j.eurpolymj.2018.04.003>
- F. Auriemma, G.C. Alfonso, C. De Rosa (eds.), *Polymer Crystallization II: From Chain Microstructure to Processing*, vol. 277 (Springer, Cham, 2017). <https://doi.org/10.1007/978-3-319-50684-5>
- I. Erukhimovich and M. O. de la Cruz, "Phase equilibria and charge fractionation in polydispersepoly electrolyte solutions," vol. 45, pp. 3003–3009 (2007). https://www.researchgate.net/publication/1944346_Phase_equilibria_and_charge_fractionation_in_polydispersepolyelectrolyte_solutions
- Q. Chen, Z. Wang, S. Zhang, Y. Cao, J. Chen, *ACS Omega* **5**(1), 655 (2020). <https://doi.org/10.1021/acsomega.9b03250>
- H. Zhou, G.L. Wilkes, *J. Mater. Sci.* **33**(2), 287 (1998). <https://doi.org/10.1023/A:1004351209140>
- R.N. Kantesh Balani, V. Verma, A. Agarwal, "Physical, Thermal, and Mechanical Properties of Polymers," in *Biosurfaces: A Materials Science and Engineering Perspective*, 1st edn. (Wiley, Hoboken, 2015), p. 329
- T. Wu, J. Xu, H. Ye, *Crystals* (Basel) **14**(3), 207 (2024). <https://doi.org/10.3390/cryst14030207>
- M.R. Mackley, *Phys. Technol.* **9**(1), 13 (1978). <https://doi.org/10.1088/0305-4624/9/1/103>
- Z. Zhang, X. Wang, Y. Wang, C. Shen, C. Liu, Z. Wang, *Polymer* (Guildford) **208**, 122875 (2020). <https://doi.org/10.1016/j.polymer.2020.122875>
- Y. Tian, C. Zhu, J. Gong, S. Yang, J. Ma, J. Xu, *Polymer* (Guildford) **55**(16), 4299 (2014). <https://doi.org/10.1016/j.polymer.2014.06.056>
- J.K. Keum, F. Zuo, B.S. Hsiao, *J. Appl. Crystallogr.* **40** (Suppl. 1), 48 (2007). <https://doi.org/10.1107/S0021889806048874>
- B.S. Hsiao, L. Yang, R.H. Somani, C.A. Avila-Orta, L. Zhu, *Phys. Rev. Lett.* **94**(11), 117802 (2005). <https://doi.org/10.1103/PhysRevLett.94.117802>
- M. An, Y. Lv, H. Xu, Y. Li, Z. Wang, *Polym. Cryst.* **2**(3) (2019). <https://doi.org/10.1002/pcr2.10060>
- K.J. Liu, J. Zhang, H. Liu, X.Y. Qian, Y. Zhang, T. Wang, K.Z. Shen, *Express Polym. Lett.* **7**(4), 355 (2013). <https://doi.org/10.3144/expresspolymlett.2013.32>
- B. Deng, L. Chen, X. Li, Z. Wang, *Macromolecules* **55**(11), 4600 (2022). <https://doi.org/10.1021/acs.macromol.2c00343>
- W. Miao, H. Zhu, T. Duan, H. Chen, F. Wu, L. Jiang, Z. Wang, *R. Soc. Open Sci.* **5**(7), 180394 (2018). <https://doi.org/10.1098/rsos.180394>
- R.H. Somani, L. Yang, L. Zhu, B.S. Hsiao, *Polymer* (Guildford) **46**(20), 8587 (2005). <https://doi.org/10.1016/j.polymer.2005.06.034>
- X.L. Xie, Y. Li, J.Z. Xu, Z. Yan, G.J. Zhong, Z.M. Li, *J. Mater. Chem. A* **6**(27), 13373 (2018). <https://doi.org/10.1039/c8ta03778g>
- C. Schaller, *4.5: Crystallinity in Polymers*, LibreTexts Chemistry (n.d.)



53. G. Li, Y. Chen, X. Tang (eds.), *Geosynthetics in Civil and Environmental Engineering: Geosynthetics Asia 2008, Proceedings of the 4th Asian Regional Conference on Geosynthetics in Shanghai, China* (Springer, Berlin, 2008)
54. B.S. Luntz, *Polymers-in-the-Mining-Industry* (AZO Mining, 2019), pp. 1–4 □

Springer Nature or its licensor (e.g. a society or other partner) holds exclusive rights to this article under a publishing agreement with the author(s) or other rightsholder(s); author self-archiving of the accepted manuscript version of this article is solely governed by the terms of such publishing agreement and applicable law.

Publisher's note

Springer Nature remains neutral with regard to jurisdictional claims in published maps and institutional affiliations.